

AperTO - Archivio Istituzionale Open Access dell'Università di Torino

Combined {DFT} and geometrical{ extendash}topological analysis of Li-ion conductivity in complex hydrides

This is the author's manuscript

Original Citation:

Availability:

This version is available <http://hdl.handle.net/2318/1755633> since 2020-09-17T17:38:10Z

Published version:

DOI:10.1039/d0qi00577k

Terms of use:

Open Access

Anyone can freely access the full text of works made available as "Open Access". Works made available under a Creative Commons license can be used according to the terms and conditions of said license. Use of all other works requires consent of the right holder (author or publisher) if not exempted from copyright protection by the applicable law.

(Article begins on next page)

Dear Author

Please use this PDF proof to check the layout of your article. If you would like any changes to be made to the layout, you can leave instructions in the online proofing interface. Making your changes directly in the online proofing interface is the quickest, easiest way to correct and submit your proof. Please note that changes made to the article in the online proofing interface will be added to the article before publication, but are not reflected in this PDF proof.

If you would prefer to submit your corrections by annotating the PDF proof, please download and submit an annotatable PDF proof by clicking [here](#) and you'll be redirected to our PDF Proofing system.

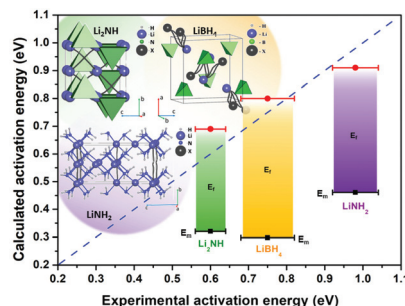
We have presented the Graphical Abstract text and image for your article below. This brief summary of your work will appear in the contents pages of the issue in which your article appears.

1

Combined DFT and geometrical–topological analysis of Li-ion conductivity in complex hydrides

Valerio Gulino, Anna Wolczyk, Andrey A. Golov, Roman A. Eremin, Mauro Palumbo,* Carlo Nervi, Vladislav A. Blatov,* Davide M. Proserpio and Marcello Baricco

This work suggests that topological analysis can adequately explain the ion conductivity in complex hydrides.



Please check this proof carefully. Our staff will not read it in detail after you have returned it.

Please send your corrections either as a copy of the proof PDF with electronic notes attached or as a list of corrections. **Do not edit the text within the PDF or send a revised manuscript** as we will not be able to apply your corrections. Corrections at this stage should be minor and not involve extensive changes.

Proof corrections must be returned as a single set of corrections, approved by all co-authors. No further corrections can be made after you have submitted your proof corrections as we will publish your article online as soon as possible after they are received.

Please ensure that:

- The spelling and format of all author names and affiliations are checked carefully. You can check how we have identified the authors' first and last names in the researcher information table on the next page. **Names will be indexed and cited as shown on the proof, so these must be correct.**
- Any funding bodies have been acknowledged appropriately and included both in the paper and in the funder information table on the next page.
- All of the editor's queries are answered.
- Any necessary attachments, such as updated images or ESI files, are provided.

Translation errors can occur during conversion to typesetting systems so you need to read the whole proof. In particular please check tables, equations, numerical data, figures and graphics, and references carefully.

Please return your **final** corrections, where possible within **48 hours** of receipt, by e-mail to: InorgChemFrontiersPROD@rsc.org. If you require more time, please notify us by email.

Funding information

Providing accurate funding information will enable us to help you comply with your funders' reporting mandates. Clear acknowledgement of funder support is an important consideration in funding evaluation and can increase your chances of securing funding in the future.

We work closely with Crossref to make your research discoverable through the Funding Data search tool (<http://search.crossref.org/funding>). Funding Data provides a reliable way to track the impact of the work that funders support. Accurate funder information will also help us (i) identify articles that are mandated to be deposited in **PubMed Central (PMC)** and deposit these on your behalf, and (ii) identify articles funded as part of the **CHORUS** initiative and display the Accepted Manuscript on our web site after an embargo period of 12 months.

Further information can be found on our webpage (<http://rsc.li/funding-info>).

What we do with funding information

We have combined the information you gave us on submission with the information in your acknowledgements. This will help ensure the funding information is as complete as possible and matches funders listed in the Crossref Funder Registry.

If a funding organisation you included in your acknowledgements or on submission of your article is not currently listed in the registry it will not appear in the table on this page. We can only deposit data if funders are already listed in the Crossref Funder Registry, but we will pass all funding information on to Crossref so that additional funders can be included in future.

Please check your funding information

The table below contains the information we will share with Crossref so that your article can be found *via* the Funding Data search tool. **Please check that the funder names and grant numbers in the table are correct and indicate if any changes are necessary to the Acknowledgements text.**

Funder name	Funder's main country of origin	Funder ID (for RSC use only)	Award/grant number
Seventh Framework Programme	European Union	100011102	ECOSTORE - 607040
Russian Science Foundation	Russia	501100006769	19-73-10026

Researcher information

Please check that the researcher information in the table below is correct, including the spelling and formatting of all author names, and that the authors' first, middle and last names have been correctly identified. **Names will be indexed and cited as shown on the proof, so these must be correct.**

If any authors have ORCID or ResearcherID details that are not listed below, please provide these with your proof corrections. Please ensure that the ORCID and ResearcherID details listed below have been assigned to the correct author. Authors should have their own unique ORCID iD and should not use another researcher's, as errors will delay publication.

Please also update your account on our online [manuscript submission system](#) to add your ORCID details, which will then be automatically included in all future submissions. See [here](#) for step-by-step instructions and more information on author identifiers.

First (given) and middle name(s)	Last (family) name(s)	ResearcherID	ORCID iD
Valerio	Gulino		
Anna	Wolczyk		
Andrey A.	Golov	H-2419-2013	0000-0002-1776-4328
Roman A.	Eremin	O-1305-2016	0000-0002-2550-9239
Mauro	Palumbo		0000-0002-0689-0839
Carlo	Nervi	B-1355-2008	0000-0002-3712-7369
Vladislav A.	Blatov	B-9962-2012	0000-0002-4048-7218

Davide M.	Proserpio	C-6391-2009	0000-0001-6597-9406
Marcello	Baricco	B-4075-2013	0000-0002-2856-9894

Queries for the attention of the authors

Journal: **Inorganic Chemistry Frontiers** Paper: **d0qi00577k**

Title: **Combined DFT and geometrical–topological analysis of Li-ion conductivity in complex hydrides**

For your information: You can cite this article before you receive notification of the page numbers by using the following format: (authors), Inorg. Chem. Front., (year), DOI: 10.1039/d0qi00577k.

Editor's queries are marked like this **Q1**, **Q2**, and for your convenience line numbers are indicated like this 5, 10, 15, ...

Please ensure that all queries are answered when returning your proof corrections so that publication of your article is not delayed.

Query Reference	Query	Remarks
Q1	Please confirm that the spelling and format of all author names is correct. Names will be indexed and cited as shown on the proof, so these must be correct. No late corrections can be made.	
Q2	Ref. 8: Please provide the initial(s) for the 6th author.	

RESEARCH ARTICLE

Combined DFT and geometrical–topological analysis of Li-ion conductivity in complex hydrides†

Cite this: DOI: 10.1039/d0qi00577k

Valerio Gulino,^{‡a} Anna Wolczyk,^{‡a} Andrey A. Golov,^b Roman A. Eremin,^{b,c} Mauro Palumbo,^{*a} Carlo Nervi,^a Vladislav A. Blatov,^{*b,c} Davide M. Proserpio^{c,d} and Marcello Baricco^a

On the basis of DFT calculations, Li-ion migration was analyzed for LiBH₄, LiNH₂, Li₂NH, Li₂BH₄NH₂, Li₄BH₄(NH₂)₃ and Li₅(BH₄)₃NH complex hydrides by means of the nudged elastic band method. In addition, a Voronoi-partition-based method, as implemented in the ToposPro program package, was adopted to determine cavities and channels in the complex hydrides and possible Li-ion migration pathways were computed. Experimental data for the Li-ion conductivity in the six compounds, measured by electrochemical impedance spectroscopy, have been taken from the literature and activation energies have been determined by a statistical analysis. A link between experimental and calculated activation energies has been evidenced, suggesting that topological analysis can provide good hints for the estimation of ion conductivity in complex hydrides.

Received 14th May 2020,
Accepted 17th July 2020
DOI: 10.1039/d0qi00577k
rsc.li/frontiers-inorganic

1. Introduction

Complex hydrides M_x(XH_n)_y (where M is a metal cation, e.g. Li⁺, and XH_n is a complex anion, e.g. [BH₄][−], [NH₂][−], [NH]^{2−}) cover a class of ionic compounds, which offers several energy-related applications, for example as potential hydrogen storage materials¹ to be used in future fuel cell technologies.² Recently, these compounds were suggested as electrolytes for all solid-state rechargeable batteries, owing not only to a high ionic conductivity coupled with a sufficient chemical and electrochemical stability, but also because of a strong compatibility with metallic Li.³

LiBH₄ shows an orthorhombic phase stable at room temperature (RT), with low Li-ion conductivity, as well as a hexagonal phase stable at temperatures higher than 110 °C, displaying superionic conductivity.⁴ Different approaches have been

applied in order to increase the Li-ion conductivity of these compounds. It can be achieved, for example, with stabilizing of the hexagonal phase by mixing it with halides^{5,6} or creating a high conductive interface by mixing or nano-confining it with oxides.^{7,8} New compounds can be also formed, as in the case of mixing LiBH₄ with lithium imide and amide.^{9,10} In the system LiBH₄–LiNH₂, two complex hydrides are stable at RT, Li₂(BH₄)(NH₂) and Li₄(BH₄)(NH₂)₃, and they exhibit lithium-ion conductivities higher than 10^{−4} S cm^{−1} at RT.^{10–12} Considering the system LiBH₄–Li₂NH, Wolczyk *et al.*⁹ reported the stability at RT of a novel compound, Li₅(BH₄)₃NH, that shows a Li-ion conductivity close to 10^{−6} S cm^{−1} at RT.

The Li-ion conductivity strictly depends on the energy barrier for diffusion, *i.e.* the minimum energy needed to complete a jump from one site to another in the crystal structure. Several approaches have recently been applied in the literature to obtain the value of this energy barrier and hence predict the ionic conductivity, such as the nudged elastic band (NEB) method,^{13–15} *ab initio* molecular dynamics (AIMD) simulations,¹⁶ or even the bond-valence (BV)¹⁷ for high-throughput pre-screening analysis.

Topological methods have also been successfully applied to reveal new prospective Li- and Na-cation conductors with oxide anionic frameworks.^{18–20} For this purpose, the combined geometrical/topological analysis, which uses the Voronoi partition of crystal space to convex polyhedra for searching for voids and channels available for mobile ions as well as the network analysis of the resulting migration map, was implemented in the

^aDepartment of Chemistry and NIS, University of Turin, Via P. Giuria 9, I-10125 Torino, Italy. E-mail: mauro.palumbo@unito.it; Fax: +39011 670 7855; Tel: +39 011 670 7097

^bSamara Center for Theoretical Materials Science, Samara University, Samara 443011, Russia

^cSamara Center for Theoretical Materials Science, Samara State Technical University, Samara 443100, Russia. E-mail: blatov@topospro.com; Fax: +7846 2784400; Tel: +7 846 3356798

^dDipartimento di Chimica, Università degli studi di Milano, 20133 Milano, Italy

†Electronic supplementary information (ESI) available. See DOI: 10.1039/d0qi00577k

‡Co-first authors.

ToposPro program package.²¹ Since the topological approach is universal, it was successfully improved and extended to new classes of materials, including complex hydrides.^{22,23}

Another route for an extension of semi-quantitative topological methods is to combine them with other simulation techniques, allowing the study of ionic transport properties at different levels of theory. We adopted the combination of experimental Solid State NMR with the computational *ab initio* modeling, namely density functional theory (DFT), to investigate the solid state properties of metal hydrides and borohydrides.^{12,24} Herein we aim to correlate ion conductivity with theoretical approaches, including the nudged elastic band (NEB) method, as implemented in various DFT packages, intended for studying energy characteristics of transition states by searching for minimum energy pathways.^{14,15}

This paper aims to provide a comprehensive study of the Li-ion transport peculiarities in LiBH_4 , LiNH_2 , Li_2NH , $\text{Li}_2\text{BH}_4\text{NH}_2$, $\text{Li}_4\text{BH}_4(\text{NH}_2)_3$ and $\text{Li}_5(\text{BH}_4)_3\text{NH}$ complex hydrides, by a combined topological–DFT approach. In this study, we apply the Voronoi-based approach for searching for spatially available Li-ion migration pathways and for the calculation of their geometrical characteristics. The pathways are then explored by the NEB method to determine migration energies barriers and to build possible migration maps for the mobile cations. In addition, we use a topological approach to identify the topological type of the migration maps obtained by the NEB method. Results on activation energy for Li-ion conductivity obtained using computational methods have been compared with those obtained experimentally in the literature, providing additional insight on the mechanisms of ion mobility in complex hydrides.

2. Methodology

The crystal structures of LiBH_4 , LiNH_2 , Li_2NH , $\text{Li}_2\text{BH}_4\text{NH}_2$, $\text{Li}_4\text{BH}_4(\text{NH}_2)_3$ and $\text{Li}_5(\text{BH}_4)_3\text{NH}$ complex hydrides have been taken from the literature, as detailed in Table S1 in ESI.†

To construct and explore migration maps for mobile Li^+ cations, we have used three methods of modeling, which are based on DFT methods, geometrical Voronoi partition and topological network approach.

2.1. DFT modeling

The method implemented in a step-by-step manner used within the current research was recently proposed and tested for solid state electrolytes.^{25,26} The relaxation (cell shape/volume and atom positions) of the available crystal structures was performed using the projector-augmented wave approach with the Perdew–Burke–Ernzerhof (PBE)²⁷ exchange–correlation functional as implemented in Vienna Ab Initio Simulation Package (VASP).²⁸ The recommended pseudopotentials were used for each chemical element. The convergences of total energy value (the tolerance of 10^{-4} eV per atom), unit cell vector length and orientation (the tolerance of 10^{-3} Å with respect to the projections of the lattice vectors) were achieved with respect

to plane-waves kinetic energy cutoff value (varying from 400 to 1000 eV with step of 200 eV) and density of the reciprocal space sampling within the Monkhorst–Pack (Γ -centered) scheme (the length parameter for automatic sampling procedure is varied from 10 to 30 Å with step of 5 Å). The energy cutoff of 600 eV and length parameter of 20 Å fitted the aforementioned convergence requirements for all systems studied.

At the next step, the optimized structures for the compounds under consideration were used for searching for migration pathways. In order to form the sets of independent Li–Li pathways, we have constructed the Voronoi partition for the Li sublattice ignoring all other atoms, as shown as an example in Fig. 1 for Li_2NH . In the Voronoi partition, each Li atom centers a convex Voronoi polyhedron, each internal point of which is closer to this Li than to other Li atoms of the sublattice. For each independent Li^+ (central) cation, we have accounted for all other $\text{Li}^+(i)$ cations, Voronoi polyhedra of which are adjacent to that of the $\text{Li}^+(\text{central})$, *i.e.* they have a common face, edge or vertex with the $\text{Li}^+(\text{central})$ Voronoi polyhedron. The longest $\text{Li}^+(\text{central})$ – $\text{Li}^+(i)$ distance defines the trusted radius, R_{trust} . Thus, the Voronoi partition was used here just to find the closest environment of a given Li^+ cation in the sublattice of mobile (Li^+) cations. Any jump of the $\text{Li}^+(\text{central})$ could be expected only to one of the neighboring Li^+ positions located inside the R_{trust} sphere that surrounds the $\text{Li}^+(\text{central})$. This approach does not fix the R_{trust} value, which can vary from one structure to another depending on the distribution of the mobile cations.

After that, each symmetry-independent pathway was modeled as a transition of Li^+ from one vacant equilibrium position to another (which corresponds to an ion–vacancy exchange) and evaluated by means of the climbing image (CI)

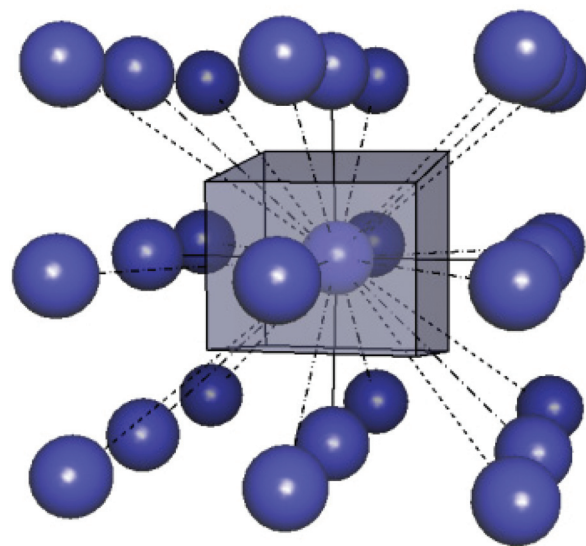


Fig. 1 The Voronoi polyhedron of a Li^+ cation in the Li sublattice of the Li_2NH crystal structure. The solid, dashed-dotted and dashed lines correspond to contacts between two Li^+ cations, which Voronoi polyhedra are adjacent by face, edge and vertex, respectively.

NEB method¹⁴ as implemented in the CP2K code.²⁹ Three-dimensional periodic boundary conditions were applied for all modeled systems. All unit cells with dimensions smaller than 8 Å were replaced by the corresponding supercells in order to exclude vacancy self-interaction. For the same reason, all the NEB runs were performed at the Γ -point of the reciprocal space.

For each pathway within the NEB modeling, eight replicas (images) were calculated using additional relaxation of the starting and ending replicas. The QuickStep³⁰ routine was used in the electron density calculations. The Goedecker-Tetter-Hutter pseudopotentials with the PBE exchange-correlation functional and the DZVP-MOLOPT-SR-GTH basis sets were chosen for all elements in the systems. The energy cutoff value of 800 Ry was applied. Three-dimensional periodic boundary conditions were applied with adding net charge of -1 electron charge value (due to Li^+ ion extraction). The tolerance on the maximum values of atom displacements and forces acting on atom of 2×10^{-4} Å and 4.5×10^{-4} Ha per Bohr, respectively, and the maximum allowed RMS values of displacements and forces of 10^{-4} Å and 3×10^{-4} Ha per Bohr were chosen as the convergence control parameters for the NEB method.

For a particular pathway, the migration energy, E_m , was evaluated as the difference between the maximal value of the corresponding energy profile and the minimal energy value among all profiles obtained for the structure under consideration. Thus, possible energy differences of crystallographically inequivalent Li-ion vacancies, as well as possible favorable intermediate positions of the mobile ion, were taken into account. At the last stage, the pathways were sorted by their E_m values to obtain the energy limits for all possible periodicities of the migration map; each limit was determined as the maximum E_m value among all pathways, which formed the map.

From the migration energies, it is possible to derive the ionic conductivity σ in an isotropic medium as described in details by Goodenough *et al.*^{31,32} For ion-vacancy conduction, Ohm's law has the form:

$$j = \sigma E = N_v N q v, \quad (1)$$

where j is the current density, E is the applied electric field, N_v and N are the numbers of vacant sites and normal sites in the lattice, respectively, q is the ion charge and v is the moving ion velocity. The ionic conductivity can be then expressed as:

$$\sigma = N_v N q u, \quad (2)$$

where $u = v/E$, *i.e.* the charge-carrier mobility. Considering the Nernst-Einstein relationship for the mobility $u = qD/k_B T$ and the Arrhenius expression for the diffusion coefficient $D = D_0 e^{-E_m/k_B T}$, and introducing them into eqn (2) we obtain:

$$\sigma = \frac{\sigma'_0}{T} e^{-E_m/k_B T}, \quad (3)$$

where $\sigma'_0 = \left(\frac{Nq^2}{k}\right) N_v D_0 e^{-\Delta S_m/k_B T}$, ΔS_m is the migration entropy and k_B is the Boltzman constant. Given the vacancy

formation energy E_f and $N_v = A e^{-E_f/k_B T}$ where A is a constant, by substituting into eqn (3) we finally obtain

$$\sigma = \frac{\sigma_0}{T} e^{-(E_m+E_f)/k_B T} = \frac{\sigma_0}{T} e^{-E_A/k_B T}, \quad (4)$$

where σ_0 is a pre-exponential factor and $E_A = E_m + E_f$ is the activation energy for ion-vacancy conduction. It can be seen that this activation energy depends both on the migration energy and the vacancy formation energy.

The latter was calculated using DFT according to the formalism detailed in by Van de Walle *et al.*³³ for a defect or impurity X in charge state q :

$$E_f[X^q] = E_{\text{tot}}[X^q] - E_{\text{tot}}[\text{perfect}] - \sum_i n_i \mu_i + q E_F, \quad (5)$$

where $E_{\text{tot}}[X^q]$ is the total energy obtained from a supercell DFT calculation with one impurity or defect X , $E_{\text{tot}}[\text{perfect}]$ is the total energy for the equivalent supercell without defects, n_i is the number of atoms of type i (host atoms or impurity) that have been added to ($n_i > 0$) or removed from ($n_i < 0$) the supercell when the defect or impurity is created and μ_i are the corresponding chemical potentials of these species. These chemical potentials represent the energy of the reservoir with which atoms are being exchange and can be determined from the experimental conditions in which the defect creation occurs. Finally, E_F is the Fermi level, also referred to as the electronic chemical potential referenced to the valence band maximum in the bulk. Note that E_F is not a free parameter, *i.e.* cannot be freely varied, but it is ultimately determined by the condition of charge neutrality. For a neutral defect ($q = 0$), it does not affect the vacancy formation energy in eqn (5).

This formalism can be applied to neutral and charged defects, vacancies and interstitial atoms and was here used to obtain the formation energies for the relevant defects, as described in the following. For these supercell calculations, the VASP code was used with the same settings as described above for the relaxation of the crystal structures, except for the k -point meshes for the reciprocal space sampling, which were appropriately reduced maintaining the same target accuracy. After introducing the defect, each supercell was relaxed with respect to the ionic positions, while keeping the cell parameters of the perfect bulk. For charged defects calculations, a compensating uniform background (jellium) is imposed to restore charge neutrality in the system.³⁴

2.2. Geometrical modeling

In the DFT approach, the migration pathways were selected among all geometrically possible jumps of Li^+ cations after relaxation of the structure in accordance with the energy criteria. To support the results obtained we applied an independent approach, which is based on the analysis of the Voronoi net, which is formed by vertices and edges of the Voronoi polyhedra of all (framework) atoms except mobile cations as shown in Fig. 2a and b for Li_2NH .¹⁸ By definition, the vertices and edges of Voronoi polyhedra represent the points of the crystal space, which are most distant from the framework

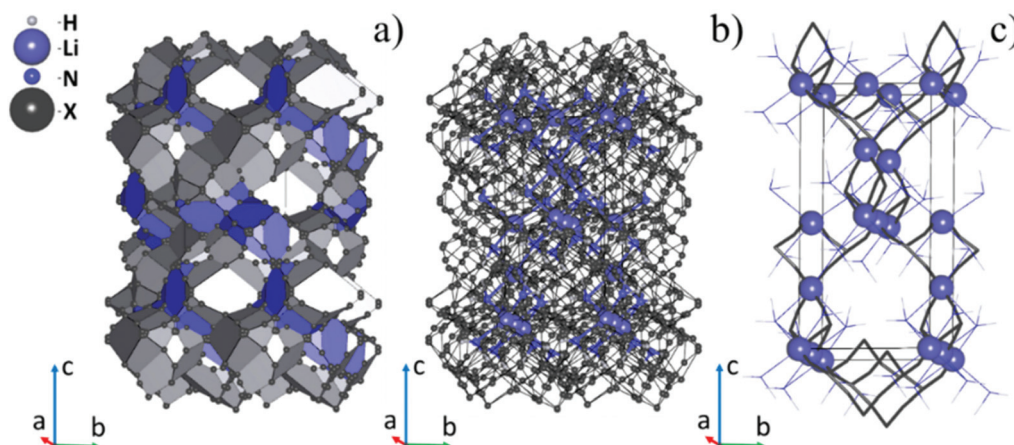


Fig. 2 (a) The Voronoi polyhedra constructed for H and N atoms in the Li_2NH structure, (b) the Voronoi net formed by vertices and edges of the atomic Voronoi polyhedra, (c) the Voronoi subnet that corresponds to the widest three-periodic channels system. The X points correspond to the vertices of the polyhedra.

atoms and, hence, mimic possible migration paths for mobile ions. This approach is somewhat opposite to the Voronoi method of searching for possible Li^+ migration paths in the DFT modeling described above. Here Li^+ cations should be excluded from consideration to leave possible migration channels free for the geometrical analysis, while in the DFT analysis only the Li^+ sublattice should be considered with the Voronoi method just to find the starting and ending points for the NEB trajectories.

At the second step, the radii of cavities and channels were evaluated. This step included the calculation of distances from nodes and edges of the Voronoi net to the closest atom, accounting for its radius; the distances reduced by the atom radius corresponded to cavities and channels radii, respectively. Since the ionic radii are not well estimated for hydrides, we used the Slater radii,³⁵ as previously applied successfully for the analysis of ion migration.^{18,19} In order to take into account lability and polarizability of structural groups, an empirical correction was applied to the radii of channels (see section 3.2). The correction obtained was then used for all complex hydrides under consideration.

The third step comprised the search for a periodic system of channels that are available for migration of mobile ions. For this purpose, all the channels and cavities of the radii, which were smaller than the radius of the mobile ion, were removed.

Further, the non-periodic (finite) systems of channels and cavities were removed. The remaining infinite channel systems were assumed to be available for migration. Additionally, the Voronoi subnets that correspond to the widest periodic channels system, available for ion migration, were found. For this purpose, the nodes and edges of the net were sorted in ascending of their radii. Then the nodes or edges of the net with a minimal value of radius (*i.e.* the narrowest part of channel) were removed. This procedure was repeated until the periodicity of the subnet decreased. The subnet of channels obtained at the previous step of the procedure was assumed the widest for the given periodicity, as shown in Fig. 2c for Li_2NH .

2.3. Topological analysis

The topological analysis of the migration maps was carried out with the ToposPro package.²¹ For this purpose, one-, two- and three-periodic nets corresponding to the lowest energy migration maps were constructed based on the results of the NEB and geometrical analyses. To identify topological type of the migration map, the corresponding net was simplified by removing one- and two-coordinated nodes and a set of topological descriptors were calculated for the simplified nets.³⁶ The topological type of the migration maps was identified by comparing the calculated set of descriptors with those from the ToposPro topological type collection (TTD). The nomenclatures of the topological types as the RCSR bold three-letter symbols (*e.g.* **sql** or **hcb**), Fischer and Koch's symbols of low-periodic sphere packings (*e.g.* $6^3(0,2)$), or ToposPro TTD symbols (*e.g.* *sqc2-7-Cmmm*) were described in detail elsewhere.^{37–39} This approach provides the information on the channels, which is essentially independent of their geometrical distortion and space group symmetry.

Thus, the three methods described above supplement each other as the geometrical approach enables one to estimate the possible positions for the NEB modeling, and the resulting NEB migration map is analyzed by the topological methods.

3. Results and discussion

3.1. Migration energy limits

After relaxation, the relative deviations of cell dimensions less than 3% with respect to the experimentally available ones were obtained and no significant crystal structure changes were observed for the compounds modeled. The resulting unit cell multiplicities, total numbers of the calculated independent pathways, distances of the longest transition, R_{trust} (in brackets) are listed in Table 1.

The calculated total energy profiles of the minimal number of independent pathways, which are required to form a three-

Table 1 The Li-ion mobility parameters obtained from DFT and ToposPro calculations

Compound		LiBH ₄	LiNH ₂	Li ₂ NH	Li ₂ NH ₂ BH ₄	Li ₄ (NH ₂) ₃ BH ₄	Li ₅ (BH ₄) ₃ NH
CI-NEB	Supercell	2 × 2 × 2	2 × 2 × 1	2 × 2 × 2	1 × 1 × 1	1 × 1 × 1	1 × 1 × 2
	Total number of pathways (R_{trust} , Å)	5 (5.43)	8 (5.148)	9 (4.35)	46 (7.932)	15 (5.712)	26 (5.870)
	Migration energy limit, eV (number of pathways in a map)	1D —	—	—	—	—	0.34 (3)
		2D 0.24 (1)	—	0.31 (2)	—	—	0.48 (6)
		3D 0.30 (2)	0.46 (2)	0.32 (3)	0.53 (5)	0.30 (2)	0.56 (10)
	The radius (Å) of the narrowest part of the widest one-, two-, or three-periodic channel systems	1D 1.214	—	1.326	1.245	—	1.387
		2D 1.168	—	—	—	—	—
		3D 1.153	1.305	1.224	1.191	1.280	1.362

“1D” symbols correspond to a certain periodicity of migration map; “—” denotes that the map with a certain periodicity is not observed.

periodic migration map, are shown in Fig. 3. The corresponding migration energy limits for certain periodicities of migration maps and numbers of the pathways involved in these maps (in brackets) are given in Table 1.

3.2. Geometrical analysis

According to the results of the NEB calculation, all considered complex hydrides possess three-periodic ionic conductivity, hence lithium cations move in a three-periodic channel system. The largest difference between Li radius (1.450 Å) and the radius of the narrowest channel in the widest three-periodic channel systems is 0.297 Å (Table 1). Thus, a value of 0.3 Å was chosen as the empirical correction of the channels radii to fit the results of the NEB calculations. This correction allows one to account for ion polarizability and relaxation of the atomic environment along the pathway during diffusion.

3.3. Topological analysis

3.3.1. LiBH₄. The LiBH₄ structure has two inequivalent lowest energy migration pathways (Fig. S1†). The pathways with the migration energy of 0.24 eV (Fig. S1a†) form a two-periodic (100) migration map with the **sql** topology (Fig. S2†). The

pathways with the migration energy of 0.30 eV form zigzag [010] chains (Fig. S1b†). The chains connect the **sql** migration layers into a three-periodic migration map of the **acs** topology (Fig. S3†).

3.3.2. LiNH₂. The LiNH₂ structure has two inequivalent Li⁺ migration pathways (Fig. S4†), which form a three-periodic migration map of the **tfa** topology (Fig. S5†). The migration map consists of (001) layers with the **sql** topology and the layers are connected by bridging pathways. The bridging pathways have the migration energy of 0.18 eV (Fig. S4a†), whereas the migration layers are formed by the pathways with a higher migration energy of 0.46 eV (Fig. S5b†).

3.3.3. Li₂NH. In the crystal structure of Li₂NH, there are three inequivalent Li⁺ migration pathways (Fig. S6†), which form the lowest energy two- (Fig. S7†) and three-periodic (Fig. S8†) migration maps. The set of the pathways with the lowest migration energy of 0.007 eV gives rise to a non-periodic migration map, which does not provide conductivity (Fig. S6a†). However, together with chain pathways [010] with the migration energy of 0.31 eV (Fig. S6b†) they form two-periodic (001) layers (Fig. S7†) with the **hcb** topology. Addition of the pathway with the migration energy of 0.32 eV (Fig. S6c†)

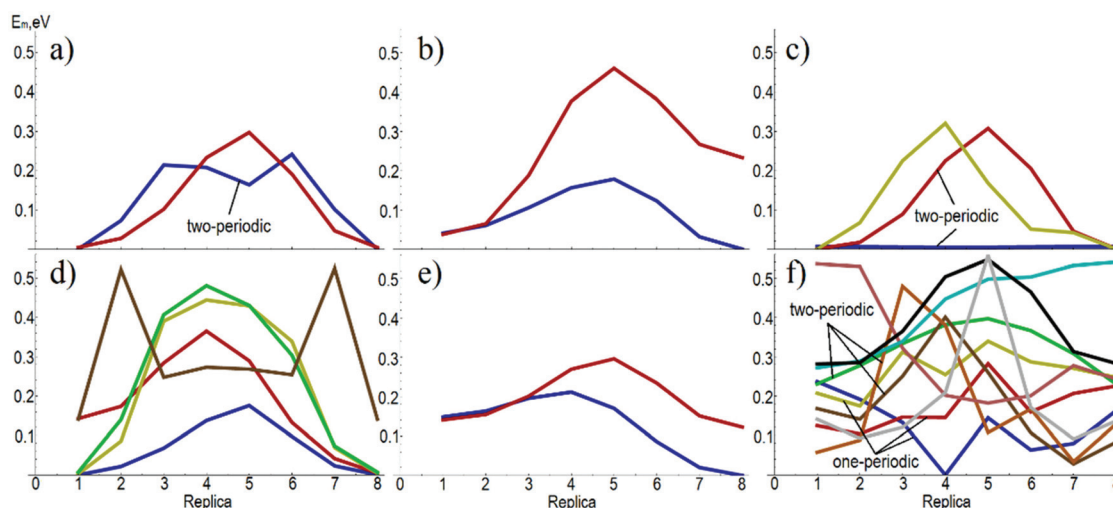


Fig. 3 The CI-NEB total energy profiles for the independent pathways, which are required to form the three-periodic migration maps in the (a) LiBH₄, (b) LiNH₂, (c) Li₂NH, (d) Li₂BH₄NH₂, (e) Li₄BH₄(NH₂)₃, and (f) Li₅(BH₄)₃NH structures. The presented profiles are obtained after subtraction of the minimum energy among the three-periodic map pathways in the given structure.

leads to a three-periodic migration map of the *sqc2-7-Cmmm* topology (Fig. S8†). It is worth noting that the latest accounted pathway individually forms two independent two-periodic (010) layers of the *sql* topology.

3.3.4. $\text{Li}_2\text{BH}_4\text{NH}_2$. The $\text{Li}_2\text{BH}_4\text{NH}_2$ structure has five inequivalent Li^+ migration pathways (Fig. S9†). Separately, each pathway does form no periodic pattern. Nevertheless, taken together they form a three-periodic migration map. The topology of the map is described by a 6-coordinated uninodal net with the $(3^{10}\cdot 8^4\cdot 9)$ point symbol (Fig. S10†).

3.3.5. $\text{Li}_4\text{BH}_4(\text{NH}_2)_3$. The $\text{Li}_4\text{BH}_4(\text{NH}_2)_3$ crystal structure has two inequivalent Li^+ migration pathways (Fig. S11†). The pathways with migration energy of 0.30 eV (Fig. S11b†) form a three-periodic migration system of the *srs* topology, while the lowest energy pathways of 0.21 eV (Fig. S11a†) are terminal (Fig. S14†) and do not influence the conductivity.

3.3.6. $\text{Li}_5(\text{BH}_4)_3\text{NH}$. The $\text{Li}_5(\text{BH}_4)_3\text{NH}$ crystal structure has a quite complicated migration system, containing ten inequivalent pathways (Fig. S13†). Three of them (Fig. S13a–c†) form an one-periodic [100] migration map of the $6^3(0,2)$ topology (Fig. S14†). Six inequivalent migration pathways (Fig. S13a–f†) form a two-periodic (010) migration map (Fig. S15†), which is characterized by a 5,6-coordinated binodal net with the $(3^2\cdot 4^5\cdot 5^4)(3^4\cdot 4^6\cdot 5\cdot 6^4)$ point symbol. The three-periodic migration map (Fig. S16†) of the topology, which is described by a three-periodic 4,7,8-coordinated three-nodal net with the $(3^2\cdot 4^4)(3^6\cdot 4^5\cdot 5^4\cdot 6^5\cdot 7)_2(3^8\cdot 4^{14}\cdot 5^6)_2$ point symbol, is formed by all ten inequivalent migration pathways.

3.4. Experimental data of Li-ion conductivity

A survey of experimental data on Li-ion conductivity reported in the literature was performed for each compound studied in this work. As experimental results of Li-ion conductivity and activation energy show significant scatter, a statistical analysis was carried out before comparison with theoretical findings, as described in ESI.† For all compounds except LiBH_4 , only a few Electrochemical Impedance Spectroscopy (EIS) measurements are reported in literature. Results of the statistical analysis are reported in Table 2.

As shown in Fig. S17,† several EIS measurements of the Li-ion conductivity of orthorhombic LiBH_4 are reported in the literature, showing a significant scatter. As an example, data span from $5 \times 10^{-8} \text{ S cm}^{-1}$ to $7 \times 10^{-7} \text{ S cm}^{-1}$ at 70 °C, within

more than an order of magnitude range. Unfortunately, details about experimental conditions regarding these measurements are often not reported in the original papers, hence results can arise from different experimental conditions and sample preparation methods.

A further experimental parameter to be considered is the application of mechanical milling. In fact, ball-milled samples show usually higher ion conductivity with respect to non-milled samples (Fig. S17†).^{40,41} The main explanation of the increased Li-ion conductivity is that the mechanochemical treatment increases the defect concentration of the orthorhombic LiBH_4 .^{7,41} The effect of ball milling on Li-ion conductivity is maintained if the sample is heated up to a temperature lower than the phase transition, as reported by Sveinbjörnsson *et al.*⁴¹ On the contrary, the higher ionic conductivity due to the mechanical milling effect is reduced after the phase transition, as reported by Matsuo *et al.*⁴⁰ and Gulino *et al.*⁷ In fact, once the milled samples undergo the phase transition, defects are recovered and the Li-ion conductivity decrease.⁷ Therefore, the data of the ball-milled samples have been excluded in the calculation of the average values reported in Table 2.

The temperature dependence of ionic conductivity σ is related to the activation energy (E_A) according to eqn (4), as described in the Methodology section. From EIS measurements reported in the literature, the activation energy (E_A) and the logarithm of the pre-exponential factor ($\ln \sigma_0$) were obtained by a linear fit of an Arrhenius plot for eqn (1), by plotting the $\ln(\sigma T)$ as a function of $1000/T$. A confidence interval was obtained from the linear fitting for both values of E_A and $\ln \sigma_0$. This interval was calculated using a confidence level of 99.99%. For each EIS measurements, the confidence level was chosen in order to include all the experimental points inside the interval, e.g. as shown in Fig. S18.†

Regarding LiBH_4 , the activation energies obtained from single set of data are reported in Table S2,† while the values of the logarithm of the pre-exponential factor are shown in Table S3.† Using the confidence interval for each EIS measurement, it was also possible to calculate a maximum and minimum value of $\ln(\sigma T)$, by using the maximum and minimum values, given by the confidence interval, of both E_A and $\ln \sigma_0$. From these values, it was possible to calculate σ at 30 °C and a confidence interval associated to it, as reported in Table S4.† For LiNH_2 , Li_2NH , $\text{Li}_2(\text{NH}_2)(\text{BH}_4)$ and $\text{Li}_4(\text{NH}_2)_3(\text{BH}_4)$ complex hydrides, both E_A and $\ln \sigma_0$ values obtained from EIS measurements reported in the literature are shown in Table S5,† whereas σ at 30 °C is reported in Table S6.†

From the statistical analysis, it was possible to obtain average values, for each compound, of the Li-ion conductivity at 30 °C, the activation energy (E_A) and the logarithm of pre-exponential factor ($\ln \sigma_0$) (Table 2). For the LiBH_4 compound, the data obtained from literature EIS measurements of ball-milled LiBH_4 , have been excluded in the calculation of the average value. Note that for $\text{Li}_5(\text{BH}_4)_3\text{NH}$ only one measurement has been reported in the literature. Therefore, the value reported in Table 2, is not an average value, but corresponds to the value associated to the single measurement reported by

Table 2 The average values of Li-ionic conductivity at 30 °C, activation energy (E_A) and $\ln \sigma_0$ obtained by the statistical analysis performed for the different investigated complex hydrides

Compound	Li-ion conductivity at 30 °C (S cm^{-1})	E_A (eV)	$\ln \sigma_0$
LiBH_4	$9.5 \times 10^{-9} \pm 2.07 \times 10^{-9}$	0.75 ± 0.07	16 ± 2
LiNH_2	$5.36 \times 10^{-11} \pm 4.11 \times 10^{-11}$	0.98 ± 0.06	19 ± 2
Li_2NH	$3.66 \times 10^{-4} \pm 8.92 \times 10^{-5}$	0.60 ± 0.04	21 ± 2
$\text{Li}_2\text{NH}_2\text{BH}_4$	$1.01 \times 10^{-4} \pm 1.63 \times 10^{-5}$	0.69 ± 0.06	23 ± 2
$\text{Li}_4(\text{NH}_2)_3\text{BH}_4$	$1.54 \times 10^{-4} \pm 4.09 \times 10^{-5}$	0.37 ± 0.02	10.1 ± 0.6
$\text{Li}_5(\text{BH}_4)_3\text{NH}$	$1.29 \times 10^{-7} \pm 8.33 \times 10^{-8}$	0.73 ± 0.03	18 ± 2

Wolczyk *et al.*⁹ In some cases, the confidence interval for E_A is >0.05 , which is relatively high compared to the corresponding values for E_A (*i.e.* up to 10%) and confirms the existence of a large scatter in experimental results from different sources.

3.5. Comparison between computed and experimental data

Possible relationships between values obtained experimentally and reported in the literature, (*e.g.* ionic conductivity at 30 °C and activation energy) and values calculated from the ToposPro output (*e.g.* channels radius and migration energy) are investigated, in order to obtain some insight into the link occurring between Li^+ ion conductivity and the topological properties of the corresponding crystal structures.

Using the data reported in Table 2, a possible relationship between channel radii (as obtained from different periodicity) and values of Li-ion conductivity at 30 °C for the series of the compounds investigated (LiBH_4 , LiNH_2 , Li_2NH , $\text{Li}_2\text{BH}_4\text{NH}_2$, $\text{Li}_4\text{BH}_4(\text{NH}_2)_3$ and $\text{Li}_5(\text{BH}_4)_3\text{NH}$) is shown in Fig. 4.

It is not possible to extract a clear trend from this figure, suggesting that the absolute value of Li-ion conductivity close to room temperature (*i.e.* at 30 °C) cannot be easily explained in terms of channel sizes in the structure. In fact, a significant contribution of the anionic species to the Li-ion conduction have been suggested for complex hydrides⁴² on the basis of the so-called “paddle-wheel” mechanism.⁴³ In fact, it should be emphasized that, although the crystal structures of $\text{Li}_2\text{BH}_4\text{NH}_2$ (*trigonal*) and $\text{Li}_4\text{BH}_4(\text{NH}_2)_3$ (*cubic*) are rather different from those of the LiBH_4 (*orthorhombic*) and LiNH_2 (*tetragonal*), the combination of anions containing hydrogen, *i.e.* $(\text{BH}_4)^-$ and $(\text{NH}_2)^-$, could provide new occupation sites for Li^+ ions, which can account for their high mobility.¹¹ LiNH_2 is characterized by a low ion mobility, because the $[\text{NH}_2]^-$ groups block the channels for Li^+ diffusion.⁴⁴

A comparison between calculated values for the migration energy and the experimental activation energy for Li-ion con-

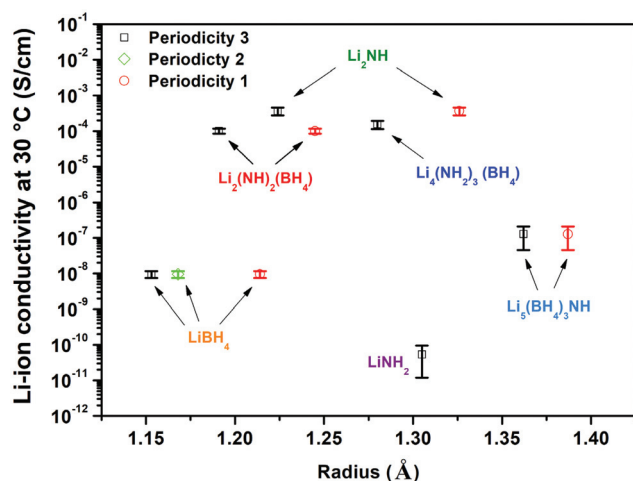


Fig. 4 Li-ion conductivity at 30 °C as a function of the radius of the narrowest part of the widest one-, two- or three-periodic channels in structures of LiBH_4 , LiNH_2 , Li_2NH , $\text{Li}_2\text{BH}_4\text{NH}_2$, $\text{Li}_4\text{BH}_4(\text{NH}_2)_3$ and $\text{Li}_5(\text{BH}_4)_3\text{NH}$.

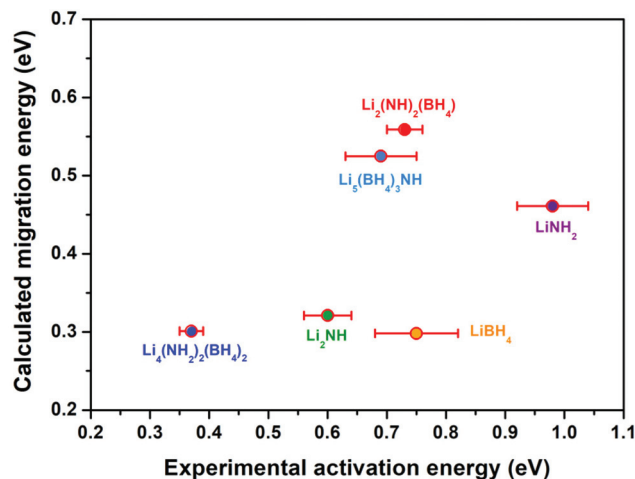


Fig. 5 Relationship between the migration energy limit calculated from DFT for LiBH_4 , LiNH_2 , Li_2NH , $\text{Li}_2\text{BH}_4\text{NH}_2$, $\text{Li}_4\text{BH}_4(\text{NH}_2)_3$, and $\text{Li}_5(\text{BH}_4)_3\text{NH}$ and activation energy determined by a statistical analysis of literature data.

ductivity is reported in Fig. 5. As already described, the activation energy was determined by statistical analysis of literature results, whereas the migration energy limit was calculated from DFT, considering both 3D and 2D periodicity, as reported in Table 1. It can be noticed that, as for the quantities shown in Fig. 4, also in this case there is no clear correlation between the calculated and experimental values, the latter being consistently and significantly higher than the calculated migration energies. The error bar associated to experimental values is large, as already pointed out, but not enough to account for the difference with computed values.

The obtained values of the E_m limits of migration maps formation (Table 1) are expected to underestimate the experimentally available E_a values, since the proposed approach does not include the energy contribution to the defect formation.

To further investigate this point, we have first analyzed theoretical results for the defect formation previously reported in the literature for the systems studied in this work (Table 3). Note that no data have been found in the literature for $\text{Li}_2\text{BH}_4\text{NH}_2$, $\text{Li}_4\text{BH}_4(\text{NH}_2)_3$, and $\text{Li}_5(\text{BH}_4)_3\text{NH}$ compounds, so the analysis has been limited to LiNH_2 , LiBH_4 and Li_2NH complex hydrides.

Calculated migration energies from the literature are also shown in Table 3 for comparison with our results and we can note that there is a satisfactory agreement between them. For example, Cho *et al.*⁵⁰ reported similar values for LiBH_4 , in the range 0.1–0.3 eV, depending on the diffusion mechanism and paths. The value of 0.3 eV reported by Hoang *et al.*⁴⁹ is matching our result. For LiNH_2 , several results are available from different authors within the range 0.20–0.46 eV, with our calculated value falling in the range, but close to the highest value.

The relevant possible defects for Li ion conduction are neutral lithium vacancies (V_{Li}), neutral lithium interstitials (Li_i) and the corresponding plus/minus one charged defects (V_{Li}^- , V_{Li}^+ , Li_i^- , Li_i^+). In all studies reported in Table 3 and in

Table 3 Defect formation and migration energies reported in the literature and calculated in this work for the considered systems. E_f is the formation energy for a single vacancy (V_{Li}^-), or equivalently for a single interstitial Li_i^+ and for a Frenkel couple (see the text for details). E_m is the migration energy of Li ions calculated in this work. Where available, the minimum distance between the vacancy and the interstitial atom in a Frenkel couple is also reported. E_A is the activation energy obtained using eqn (4). Note that the formation energy of Frenkel pair with finite distance (or not reported in the original paper) do not equal two times the formation energy of a single defect

Compound	Ref.	$E_f Li_i^+$ or V_{Li}^- (eV)	E_f Frenkel pair (eV)	Min. distance (Frenkel pair)	E_m (eV)	E_A (eV)
LiNH ₂	45	0.51	0.65	0.85 Å	0.2–0.3	0.71–0.81
	46	0.57	0.72	—	0.46	1.03
	47	0.52	0.79	—	0.44	0.96
	48	0.49 ^a	0.97	—	0.22–0.42	0.71–0.91
	44	—	—	—	0.38	—
LiBH ₄	Present work	0.45	0.90	∞	0.46	0.91
	49	0.5	0.95	4.2 Å	0.3	0.8
	50	0.6 ^a	1.2	∞	0.1–0.3	0.7–0.9
			0.88	4 Å		
Li ₂ NH	Present work	0.5	1.0	∞	0.30	0.80
	44	0.24 ^a	0.48	—	0.17–0.47	0.41–0.71
	Present work	0.37	0.74	∞	0.32	0.69

^a Calculated dividing by 2 the E_f Frenkel pair.

the present work, the combination of V_{Li}^- and Li_i^+ , also known as a Frenkel pair, has been found to be the most stable. We then assume this as a common mechanism for all examined compounds. Regarding the defect formation energies, it is worth noting that different approaches can be used to obtain such energies from the DFT calculations. For example, most of the values in Table 3 have been calculated following an approach proposed by Van de Walle *et al.*,³³ which has been described in the Methodology section and used in our own calculations. This method has been used in ref. 44–49. According to this approach, the formation energy of a single charged isolated defect can be plotted as a function of the Fermi level as in eqn (5). It has already pointed out, however, that this Fermi level is not a free parameter.³³ In a real system, in fact, the charge balance must be maintained, *i.e.* charged defects form as pairs, such as Frenkel pairs (V_{Li}^- , Li_i^+). The formation energies of V_{Li}^- and Li_i^+ , calculated in eqn (5) as a function of E_F , cross at a given Fermi level and the crossing point represents their formation energies in the real system. As a consequence, the formation energies of V_{Li}^- and Li_i^+ are the same and their sum gives the formation energy of the Frenkel pair at infinite distance, *i.e.* for isolated defects.

Another approach can be used for computing the formation energy of defect pairs, such as Frenkel or Schottky couples. Note that the formation energy of Frenkel or Schottky pairs can be obtained from the formation energies of single defects. The formation of such couples maintains the electrical neutrality of the crystal and there is no need to add correction terms and reservoirs. Hence, formation energies are simply obtained as difference between the total energies of supercells with and without defects. However, several possible crystallographic sites must be considered, where, for example, the interstitial atom in a Frenkel couple can move from its lattice position. Different distances between the interstitial atom and the vacancy are thus obtained and the formation energy can be obtained by extrapolation at infinite distance. Cho *et al.*⁵⁰

reported the results for the formation energy of Frenkel defect pairs in LiBH₄ using this approach.

Note that for LiNH₂, several theoretical values are available, and a certain scatter can be observed in Table 3. As different computational parameters and program codes were used, it is difficult to clearly identify possible reasons for these differences, which can be considered as differences in the experimental measurements. Note also that, in some cases,^{45,49,50} a specific distance was assumed between the vacancy and the interstitial in the Frenkel couple, which may account for part of the discrepancies found.

In order to estimate the activation energy, the energies of formation for V_{Li}^- calculated in this work (Table 3) have been

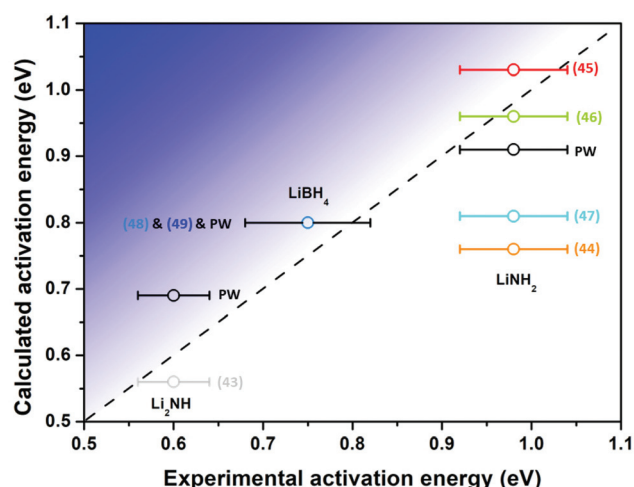


Fig. 6 Activation energy calculated as a function of the values obtained from the statistical analysis of literature data, where different colors indicates different references, PW ("present work") indicates the data calculated in this work. The dashed line is a guide for the eyes to show the correspondence of calculated and experimental values.

added to the calculated migration energy (Tables 1 and 3) according to eqn (4), and the results are reported in the last column in Table 3.

A comparison between computed and experimental values for the activation energy for LiNH_2 , LiBH_4 and Li_2NH complex hydrides is shown in Fig. 6. A satisfactory correspondence between theoretical and experimental values can now be observed when considering the experimental error bar. Despite the large scatter observed in both experimental and theoretical values, it appears reasonable to confirm that the Li-ion conduction mechanism theoretically considered in this work is realized in the complex hydrides.

4. Conclusions

We have obtained the energy limits of a certain migration map periodicities with DFT calculations by means of the NEB method for the LiBH_4 , Li_2NH , $\text{Li}_2\text{BH}_4\text{NH}_2$, $\text{Li}_4\text{BH}_4(\text{NH}_2)_3$ and $\text{Li}_5(\text{BH}_4)_3\text{NH}$ structures. The sets of the energetically favorable migration pathways were subsequently analyzed in relation to their topologies and compared with the results of the geometrical search for migration channels. The geometrical/topological analysis of the migration pathways was performed using Voronoi partition method, which was adopted to determine cavities and channels in the structure of considered complex hydrides. It was shown that the topology of the lowest energy migration map obtained by the NEB calculations is in a good correlation with the Voronoi analysis. In addition, a statistical analysis of the literature data has been performed for each compound in order to obtain the average values for the activation energy, $\ln \sigma_0$ and Li-ion conductivity at 30 °C. A correlation between the experimental and calculated values for Li-ion mobility has been evidenced for LiNH_2 , LiBH_4 and Li_2NH complex hydrides, suggesting that the topological analysis can adequately explain the ion conductivity in complex hydrides. Authors believe that the further development of the proposed combined approach concerning other migration mechanisms or defect influence on the ionic transport properties might be of high importance for its future applications.

Conflicts of interest

Authors have no competing interests to declare.

Acknowledgements

European Marie Curie Actions under ECOSTORE grant agreement no. 607040 is acknowledged for supporting this work. The work on the geometrical/topological analysis and DFT calculations of migration barriers was supported by the Russian Science Foundation (project 19-73-10026). We are also obliged to computational facilities of the Samara University computing complexes 'Sergey Korolev' and 'Zeolite' (Samara Center for Theoretical Materials Science).

References

- 1 D. Pottmaier, E. R. Pinatel, J. G. Vitillo, S. Garroni, M. Orlova, M. D. Baró, G. B. M. Vaughan, M. Fichtner, W. Lohstroh and M. Baricco, Structure and Thermodynamic Properties of the NaMgH_3 Perovskite: A Comprehensive Study, *Chem. Mater.*, 2011, **23**, 2317–2326.
- 2 P. P. Edwards, V. L. Kuznetsov, W. I. F. David and N. P. Brandon, Hydrogen and Fuel Cells: Towards a Sustainable Energy Future, *Energy Policy*, 2008, **36**, 4356–4362.
- 3 X. Luo, J. Wang, M. Dooner and J. Clarke, Overview of Current Development in Electrical Energy Storage Technologies and the Application Potential in Power System Operation, *Appl. Energy*, 2015, **137**, 511–536.
- 4 M. Matsuo, Y. Nakamori, S. Orimo, H. Maekawa and H. Takamura, Lithium Superionic Conduction in Lithium Borohydride Accompanied by Structural Transition, *Appl. Phys. Lett.*, 2007, **91**, 224103.
- 5 D. Sveinbjörnsson, A. S. Christiansen, R. Viskinde, P. Norby and T. Vegge, The LiBH_4 -LiI Solid Solution as an Electrolyte in an All-Solid-State Battery, *J. Electrochem. Soc.*, 2014, **161**(9), A1432–A1439.
- 6 V. Gulino, M. Brighi, E. M. Dematteis, F. Murgia, C. Nervi, R. Černý and M. Baricco, Phase Stability and Fast Ion Conductivity in the Hexagonal LiBH_4 -LiBr-LiCl Solid Solution, *Chem. Mater.*, 2019, **31**, 5133–5144.
- 7 V. Gulino, L. Barberis, P. Ngene, M. Baricco and P. E. de Jongh, Enhancing Li-Ion Conductivity in LiBH_4 -Based Solid Electrolytes by Adding Various Nanosized Oxides, *ACS Appl. Energy Mater.*, 2020, **3**, 4941–4948.
- 8 D. Blanchard, A. Nale, D. Sveinbjörnsson, T. M. Eggenhuisen, M. H. W. Verkuijen, Suwarno, T. Vegge, A. P. M. Kentgens and P. E. de Jongh, Nanoconfined LiBH_4 as a Fast Lithium Ion Conductor, *Adv. Funct. Mater.*, 2015, **25**, 184–192.
- 9 A. Wolczyk, B. Paik, T. Sato, C. Nervi, M. Brighi, S. P. GharibDoust, M. Chierotti, M. Matsuo, G. Li, R. Gobetto, T. R. Jensen, R. Černý, S. Orimo and M. Baricco, $\text{Li}_5(\text{BH}_4)_3\text{NH}$: Lithium-Rich Mixed Anion Complex Hydride, *J. Phys. Chem. C*, 2017, **121**, 11069–11075.
- 10 Y. Zhou, M. Matsuo, Y. Miura, H. Takamura, H. Maekawa, A. Remhof, A. Borgschulte, A. Züttel, T. Otomo and S. Orimo, Enhanced Electrical Conductivities of Complex Hydrides $\text{Li}_2(\text{BH}_4)(\text{NH}_2)$ and $\text{Li}_4(\text{BH}_4)(\text{NH}_2)_3$ by Melting, *Mater. Trans.*, 2011, **52**, 654–657.
- 11 M. Matsuo, A. Remhof, P. Martelli, R. Caputo, M. Ernst, Y. Miura, T. Sato, H. Oguchi, H. Maekawa, H. Takamura, A. Borgschulte, A. Züttel and S. Orimo, Complex Hydrides with $(\text{BH}_4)^-$ and $(\text{NH}_2)^-$ Anions as New Lithium Fast-Ion Conductors, *J. Am. Chem. Soc.*, 2009, **131**, 16389–16391.
- 12 A. Wolczyk, E. R. Pinatel, M. R. Chierotti, C. Nervi, R. Gobetto and M. Baricco, Solid-State NMR and Thermodynamic Investigations on $\text{LiBH}_4\text{LiNH}_2$ System, *Int. J. Hydrogen Energy*, 2016, **41**, 14475–14483.
- 13 F. T. Bølle, N. R. Mathiesen, A. J. Nielsen, T. Vegge, J. M. Garcia-Lastra and I. E. Castelli, Autonomous

- Discovery of Materials for Intercalation Electrodes, *Batteries Supercaps*, 2020, **3**, 488–498.
- 14 G. Henkelman, B. P. Uberuaga and H. Jónsson, A Climbing Image Nudged Elastic Band Method for Finding Saddle Points and Minimum Energy Paths, *J. Chem. Phys.*, 2000, **113**, 9901–9904.
- 15 S. Shi, J. Gao, Y. Liu, Y. Zhao, Q. Wu, W. Ju, C. Ouyang and R. Xiao, Multi-Scale Computation Methods: Their Applications in Lithium-Ion Battery Research and Development, *Chin. Phys. B*, 2016, **25**, 018212.
- 16 Z. Deng, Z. Zhu, I.-H. Chu and S. P. Ong, Data-Driven First-Principles Methods for the Study and Design of Alkali Superionic Conductors, *Chem. Mater.*, 2017, **29**, 281–288.
- 17 R. Xiao, H. Li and L. Chen, Candidate Structures for Inorganic Lithium Solid-State Electrolytes Identified by High-Throughput Bond-Valence Calculations, *J. Materiomics*, 2015, **1**, 325–332.
- 18 N. A. Anurova, V. A. Blatov, G. D. Ilyushin, O. A. Blatova, A. K. Ivanov-Schitz and L. N. Dem'yanets, Migration Maps of Li^+ cations in Oxygen-Containing Compounds, *Solid State Ionics*, 2008, **179**, 2248–2254.
- 19 F. Meutzner, W. Münchgesang, N. A. Kabanova, M. Zschornak, T. Leisegang, V. A. Blatov and D. C. Meyer, On the Way to New Possible Na-Ion Conductors: The Voronoi-Dirichlet Approach, Data Mining and Symmetry Considerations in Ternary Na Oxides, *Chem. – Eur. J.*, 2015, **21**, 16601–16608.
- 20 M. Brighi, P. Schouwink, Y. Sadikin and R. Černý, Fast Ion Conduction in Garnet-Type Metal Borohydrides $\text{Li}_{13}\text{K}_3\text{Ce}_2(\text{BH}_4)_{12}$ and $\text{Li}_3\text{K}_3\text{La}_2(\text{BH}_4)_{12}$, *J. Alloys Compd.*, 2016, **662**, 388–395.
- 21 V. A. Blatov, A. P. Shevchenko and D. M. Proserpio, Applied Topological Analysis of Crystal Structures with the Program Package ToposPro, *Cryst. Growth Des.*, 2014, **14**, 3576–3586.
- 22 S. H. P. GharibDoust, M. Brighi, Y. Sadikin, D. B. Ravnsbæk, R. Černý, J. Skibsted and T. R. Jensen, Synthesis, Structure, and Li-Ion Conductivity of $\text{LiLa}(\text{BH}_4)_3\text{X}$, $\text{X} = \text{Cl}, \text{Br}, \text{I}$, *J. Phys. Chem. C*, 2017, **121**, 19010–19021.
- 23 E. Didelot and R. Černý, Ionic Conduction in Bimetallic Borohydride Borate, $\text{LiCa}_3(\text{BH}_4)(\text{BO}_3)_2$, *Solid State Ionics*, 2017, **305**, 16–22.
- 24 F. Franco, M. Baricco, M. R. Chierotti, R. Gobetto and C. Nervi, Coupling Solid-State NMR with GIPAW Ab Initio Calculations in Metal Hydrides and Borohydrides, *J. Phys. Chem. C*, 2013, **117**, 9991–9998.
- 25 R. A. Eremin, N. A. Kabanova, Y. A. Morkhova, A. A. Golov and V. A. Blatov, High-Throughput Search for Potential Potassium Ion Conductors: A Combination of Geometrical-Topological and Density Functional Theory Approaches, *Solid State Ionics*, 2018, **326**, 188–199.
- 26 R. A. Eremin, P. N. Zolotarev, A. A. Golov, N. A. Nekrasova and T. Leisegang, Ionic Transport in Doped Solid Electrolytes by Means of DFT Modeling and ML Approaches: A Case Study of Ti-Doped KFeO_2 , *J. Phys. Chem. C*, 2019, **123**, 29533–29542.
- 27 J. P. Perdew, K. Burke and M. Ernzerhof, Generalized Gradient Approximation Made Simple, *Phys. Rev. Lett.*, 1996, **77**, 3865–3868.
- 28 G. Kresse and J. Furthmüller, Efficient Iterative Schemes for Ab Initio Total-Energy Calculations Using a Plane-Wave Basis Set, *Phys. Rev. B: Condens. Matter Mater. Phys.*, 1996, **54**, 11169–11186.
- 29 J. Hutter, M. Iannuzzi, F. Schiffmann and J. VandeVondele, CP2K: Atomistic Simulations of Condensed Matter Systems, *Wiley Interdiscip. Rev.: Comput. Mol. Sci.*, 2014, **4**, 15–25.
- 30 J. VandeVondele, M. Krack, F. Mohamed, M. Parrinello, T. Chassaing and J. Hutter, Quickstep: Fast and Accurate Density Functional Calculations Using a Mixed Gaussian and Plane Waves Approach, *Comput. Phys. Commun.*, 2005, **167**, 103–128.
- 31 J. B. Goodenough, Review Lecture: Fast Ionic Conduction in Solids, *Proc. R. Soc. A*, 1984, **393**, 215–234.
- 32 J. B. Goodenough, Oxide-Ion Electrolytes, *Annu. Rev. Mater. Res.*, 2003, **33**, 91–128.
- 33 C. G. Van de Walle and J. Neugebauer, First-Principles Calculations for Defects and Impurities: Applications to III-Nitrides, *J. Appl. Phys.*, 2004, **95**, 3851–3879.
- 34 C. G. Van de Walle, P. J. H. Denteneer, Y. Bar-Yam and S. T. Pantelides, Theory of Hydrogen Diffusion and Reactions in Crystalline Silicon, *Phys. Rev. B: Condens. Matter Mater. Phys.*, 1989, **39**, 10791–10808.
- 35 J. C. Slater, Atomic Radii in Crystals, *J. Chem. Phys.*, 1964, **41**, 3199–3204.
- 36 V. A. Blatov, M. O'Keeffe and D. M. Proserpio, Vertex-, Face-, Point-, Schläfli-, and Delaney-Symbols in Nets, Polyhedra and Tilings: Recommended Terminology, *CrystEngComm*, 2010, **12**, 44–48.
- 37 E. Koch and W. Z. Fischer, Types of Sphere Packings for Crystallographic Point Groups, Rod Groups and Layer Groups, *Z. Kristallogr.*, 1978, **148**, 107–152.
- 38 M. O'Keeffe, M. A. Peskov, S. J. Ramsden and O. M. Yaghi, The Reticular Chemistry Structure Resource (RCSR) Database of, and Symbols for, Crystal Nets, *Acc. Chem. Res.*, 2008, **41**, 1782–1789.
- 39 V. A. Blatov, E. V. Alexandrov and A. P. Shevchenko, Topology: ToposPro, in *Reference Module in Chemistry, Molecular Sciences and Chemical Engineering*, Elsevier, 2019, pp. 1–23.
- 40 M. Matsuo, H. Takamura, H. Maekawa, H.-W. Li and S. Orimo, Stabilization of Lithium Superionic Conduction Phase and Enhancement of Conductivity of LiBH_4 by LiCl Addition, *Appl. Phys. Lett.*, 2009, **94**, 084103.
- 41 D. Sveinbjörnsson, D. Blanchard, J. S. G. Myrdal, R. Younesi, R. Viskinde, M. D. Riktor, P. Norby and T. Vegge, Ionic Conductivity and the Formation of Cubic CaH_2 in the $\text{LiBH}_4\text{--Ca}(\text{BH}_4)_2$ Composite, *J. Solid State Chem.*, 2014, **211**, 81–89.
- 42 P. Martelli, A. Remhof, A. Borgschulte, R. Ackermann, T. Strässle, J. P. Embs, M. Ernst, M. Matsuo, S.-I. Orimo and A. Züttel, Rotational Motion in LiBH_4/LiI Solid Solutions, *J. Phys. Chem. A*, 2011, **115**, 5329–5334.

- 43 M. Jansen, Volume Effect or Paddle-Wheel Mechanism—Fast Alkali-Metal Ionic Conduction in Solids with Rotationally Disordered Complex Anions, *Angew. Chem., Int. Ed. Engl.*, 1991, **30**, 1547–1558.
- 44 W. Li, G. Wu, Z. Xiong, Y. P. Feng and P. Chen, Li⁺ Ionic Conductivities and Diffusion Mechanisms in Li-Based Imides and Lithium Amide, *Phys. Chem. Chem. Phys.*, 2012, **14**, 1596–1606.
- 45 K. Hoang, A. Janotti and C. G. Van De Walle, The Particle-Size Dependence of the Activation Energy for Decomposition of Lithium Amide, *Angew. Chem., Int. Ed.*, 2011, **50**, 10170–10173.
- 46 E. Hazrati, G. Brocks, B. Buurman, R. A. De Groot and G. A. De Wijs, Intrinsic Defects and Dopants in LiNH₂: A First-Principles Study, *Phys. Chem. Chem. Phys.*, 2011, **13**, 6043–6052.
- 47 J. Wang, Y. Du, H. Xu, C. Jiang, Y. Kong, L. Sun and Z. K. Liu, Native Defects in LiNH₂: A First-Principles Study, *Phys. Rev. B: Condens. Matter Mater. Phys.*, 2011, **84**, 21–24.
- 48 G. Miceli, C. S. Cucinotta, M. Bernasconi and M. Parrinello, First Principles Study of the LiNH₂/Li₂NH Transformation, *J. Phys. Chem. C*, 2010, **114**, 15174–15183.
- 49 K. Hoang and C. G. Van De Walle, Mechanism for the Decomposition of Lithium Borohydride, *Int. J. Hydrogen Energy*, 2012, **37**, 5825–5832.
- 50 Y.-S. Lee and Y. W. Cho, Fast Lithium Ion Migration in Room Temperature LiBH₄, *J. Phys. Chem. C*, 2017, **121**, 17773–17779.